

ORIGINAL RESEARCH

## Modelling and optimization of *luffa* oil transesterification via acid activated waste marble catalyst

Maureen A. Allen<sup>1</sup>, Kenechi Nwosu-Obieogu<sup>2,\*</sup>, Chukwunonso N. Nwogu<sup>1</sup>, Berthrand Nwankwojike<sup>1</sup>, Simeon Bright<sup>1</sup>, Christian Goodnews<sup>2</sup>

Received: 22nd July, 2023 / Accepted: 8th February, 2024

Published online: 30th March, 2024

### Abstract

This study assessed the performance of response surface methodology (RSM) and artificial neural network (ANN) in modelling the transesterification of *luffa* oil using acid activated waste marble catalyst. The waste marble was activated with 0.5 molar sulphuric acid at 600 °C for 4 hours and was characterized by SEM, FT-IR, XRD, XRF, and BET; the characterization proved that the catalyst was successfully activated. The experiments were conducted at a catalyst dosage (1-5 wt. %), temperature (40-80 °C), methanol-oil ratio (4:1-12:1), time (1-3 hours), and agitation speed of (100- 500 rpm) with output as biodiesel yield. ANN was assessed using three back-propagation (BP) procedures, each comprising five neurons (input layer), one (output layer) and ten (hidden layer). The Levenberg Marquardt technique offered the most accurate prediction for *luffa* oil transesterification. The models were developed based on experimental and algorithm simulations and designs. The models' performance was assessed using the R<sup>2</sup> and MSE. Regarding R<sup>2</sup> and MSE, the ANN model (R<sup>2</sup>=9.9921E-1, MSE=0.06311) has a superior predictive capacity in forecasting the process than the RSM (R<sup>2</sup>=0.9885, MSE=0.86). At a catalyst concentration (3wt %), time (2 hours), temperature (60 °C), agitation speed (100 rpm) and methanol-oil ratio (12:1), the experimental (92.57 %), RSM predicted (94.0487 %) and ANN predicted (91.1768 %) biodiesel yield showed an agreement between the experimental and predicted values. The findings via physicochemical analysis, FT-IR, and GC-MS confirm that the biodiesel was within ASTM specifications.

**Keywords:** *Luffa* Oil, Transesterification, Biodiesel, Optimization

### Introduction

Dependence on energy resources is vital for economic development in the world. However, fossil fuels pose adverse environmental and deteriorating effects on the atmosphere, so the need to exploit renewable sources of fuel becomes paramount (Ude *et al.*, 2017); biodiesel, a renewable source of fuel, is receiving attention from researchers because of its fuel properties and compatibility; it also has better properties than petrodiesel such as renewability, higher biodegradability, excellent lubricity, and clean combustion (Abdul Mutalib *et al.*, 2020; Peighambardoust *et al.*, 2021).

Plant oils are the most widely utilised feedstocks for the production of biodiesel; within vegetable oils, inedible oils are preferred due to their non-competitiveness with food and availability, and it grows with little stress (Idris *et al.*, 2021; Sahu, 2021). *Luffa* oil is an inedible oil obtained from *luffa* plants. It is an annual plant found in the tropics, belongs to the vast *Cucurbitaceae* plant and is generally regarded as a non-economical viable material (Chinweuba, 2017). Reports have shown that *luffa* oil is valuable potential for transesterification due to its oleic, linoleic, and linolenic acid content (Nwosu-obieogu and Umunna, 2021). Few researchers have reported on *luffa* oil utilization for the production of biofuel such as; Ibeta *et al.* (2012) characterized *luffa* oil for the production of biodiesel; their findings revealed that it contains unsaturated triglycerides which makes it suitable for the process; Adewuyi *et al.* (2012) also opined that *luffa* oil contains high FFA that will be esterified before transesterification process. Oniya and Bamgboye (2012) studied the biodiesel properties of *luffa* oil,

and it has good fuel quality compared to the ASTM standard for diesel engine fuels.

The drawbacks of the homogeneous catalysed process, such as inefficient catalyst separation, by-product removal, catalyst corrosiveness, and reaction with FFA resulting in soap formation, have been mitigated by using a catalyst of heterogeneous nature (Nwosu-obieogu *et al.*, 2023). Additionally, the utilization of heterogeneous catalysts in the process, which are primarily obtained from wastes leads to reduced production costs (Nadeem *et al.*, 2021; Onukwuli *et al.*, 2023).

Marble waste is valued as a high-quality catalyst because of its strong and lasting nature, alkaline properties, and capacity to fully dissolve in alcohol. Its primary component is Calcium oxide (CaO) (Abdul Mutalib *et al.*, 2020). Several papers demonstrate the utilization of calcined waste marble slurry and hydroxyapatite catalyst in soya bean oil biodiesel production, with improved catalyst reusability (Laskar *et al.*, 2020). Bedir and Dogan (2021) calcined waste marble for sunflower biodiesel transesterification process, and the waste marble dust showed high catalytic activity by actualizing (89.14 %) FAME yield. Khan *et al.* (2019) successfully synthesized methyl ester from waste oil via a waste marble catalyst. Gupta *et al.* (2023) successfully applied waste marble powdered heterogeneous catalysts for production of methyl ester from *Pongamia pinnata* oil and inferred the stability and high activity of the catalyst.

The issues associated with one factor at a time in the analysis, such as the expensiveness and limited information concerning the interaction and quadratic terms of variable, model development, and optimization, have led to the introduction of RSM (Shobhana-Gnanaserkhar *et al.*, 2020). The RSM can be applied to optimize the chemical process within a limited time (Ajala *et al.*, 2015; Balajii and Niju, 2020; Foroutan, Peighambardoust *et al.*, 2021). Several researchers have applied RSM in transesterification process modelling using activated waste marble catalysts; the optimization of

\*Corresponding author: kenenwosuobie@mouau.edu.ng

<sup>1</sup>Mechanical Engineering Department, Michael Okpara University of Agriculture, Umudike, Abia, Nigeria.

<sup>2</sup>Chemical Engineering Department, Michael Okpara University of Agriculture, Umudike, Abia, Nigeria.

waste oil biodiesel using waste marble powder by Bargole *et al.* (2021) with a yield of 95.45 % was obtained at 180 minutes, alcohol to oil ratio of 15.9:1, temperature of 64.8 °C and catalyst dosage of 6.8 wt%.

However, RSM's incapacity to simulate sophisticated and nuanced processes has prompted the creation of soft computing models. Artificial Neural Networks are effective data-driven modelling techniques that excel at capturing complex non-linear behaviours due to their high generalization structure. They were inspired by biological neural systems and are commonly applied for complex modelling, and identification. (Oke *et al.*, 2021). RSM has been applied in various inedible oil transesterification processes such as production of methyl ester from waste fat (Foroutan *et al.*, (2021), engine performance prediction of African pear oil biodiesel (Esonye *et al.*, 2019), biodiesel production via fluorite heterogeneous catalyst prediction (Sai *et al.* 2019) and methyl ester yield from pig tallow (Suresh *et al.*, 2021). Nevertheless, no information has been reported on ANN and RSM application to model the *luffa* oil transesterification process; thus, this work applies ANN and RSM to model the *luffa* oil transesterification process.

## Materials and Methods

### Materials and preparation of catalyst

*Luffa* oil was obtained from *luffa cylindrica* seeds via solvent extraction whereas chemicals and waste marble were obtained from construction sites where they were dumped. All the chemicals utilized in the study were of analytical grade and needed no purification further.

The waste marble was blended and sieved to get the powdered form of it, and it was calcinated at 600 °C for 4 hours. It was then treated with 0.5 M sulphuric acid. The acid-activated marble was characterized by different techniques such as basicity test, acidic test, qualitative analysis, FTIR, SEM, XRF, and XRD. The acid-activated waste marble was submerged in a 30 % hydrogen peroxide solution in a 1:2 weight-to-weight ratio at 30 °C for 24 hours to remove contaminants. To eliminate excess H<sub>2</sub>O<sub>2</sub>, the mixture was slowly heated in a water bath before being removed from the clay. The washed clay was then suspended in distilled water at a 1:4 weight-to-weight ratio and given time to settle. It was then sieved and oven dried at 110 °C to remove the moisture content. The marble was grinded and put through an 80/100 grit filter. Sulphuric acid activation was used to remove extra salt from the dried waste marble catalyst and increase activity. Approximately 0.5 M solution of sulphuric acid was combined with the dried sample in a ratio of 1:1. The reaction was conducted for two hours at 100 °C with vigorous stirring in a flask. A reflux condenser and glycerine bath were used to heat the process. The acid-activated waste marble was washed until its pH was about 7, and it was then dried for six hours at 110 °C.

### Waste marble characterization

Morphology of the waste marble samples was determined using SEM and XRF to analyse the elemental constituents, FT-IR for functional group determination, and XRD to assess the waste marble structural composition and crystallinity. Average pore diameter, surface area and total pore volume of the waste marble were determined by BET analysis. A micrometric ASAP 2020 surface analyser calculated the pore volume, pore diameter, and surface area from N<sub>2</sub> adsorption isotherms.

### *luffa* oil characterization

The physicochemical characterization of *luffa* oil was evaluated following AOAC methods. The *luffa* oil was characterized by determining the saponification, acid and iodine value, free fatty acid, kinematic viscosity, density, ester, moisture, peroxide value and refractive index .

### FT-IR

FTIR techniques were complementary methods (after chemical processes) to characterize structural functionalities in the pure and transesterified *luffa seed* oil (LSO). FTIR spectrum of the transesterified oil was recorded with a Shimadzu 8400SFTIR spectrophotometer over the range 4500 – 350cm<sup>-1</sup> using ten scans at a resolution of 4cm<sup>-1</sup>.

### GC-MS

GC-MS analysis of the pure and transesterified samples involved mixing 50 mg of the sample in 10 mL of toluene with 0.2 mL of Tetramethylammonium hydroxide (TMAH) by shaking. 4mL of water was added to the mixture, which was then allowed to settle. The samples were examined for their fatty acid profiles. The peaks were detected using a Mass Spectrometer connected to a Gas Chromatography-Mass Spectrometry system.

### Transesterification procedure

When exposed to acid-activated waste marble, *luffa* oil undergoes a reaction with methanol to produce glycerol and biodiesel. The oil was transferred into a flask using a heated magnetic stirrer. The methanol was then mixed with catalyst. The reaction flask was placed on a heated stirrer at a constant temperature during the reaction. The sample was withdrawn after the prescribed time, while methyl ester, and by-product (glycerol) settled at room temperature in a separating funnel. The yield percentage was calculated by comparing the vol. of the biodiesel to the vol. of oil used, as per Equation (1).

$$\text{Yield (\%)} = \frac{\text{weight of methyl ester}}{\text{oil weight}} \times 100 \quad (1)$$

### Design of experiment

A Box-Behnken design with 5 factors and a 3-level base was created via Design-Expert software for the experiment. The study measured the methyl ester yield as the main outcome, with the catalyst dosage, temperature, methanol-oil molar ratio, time, and speed of agitation as the variables. Table 1 displays the design summary

**Table 1** Design summary

Name	Units	Type	Level		
			-1	0	1
Catalyst concentration	mol	Numeric	1	3	5
Methanol/oil molar ratio		Numeric	4	8	12
Time	Hour	Numeric	1	2	3
temperature	°C	Numeric	40	60	80
Agitation speed	rpm	Numeric	100	300	500

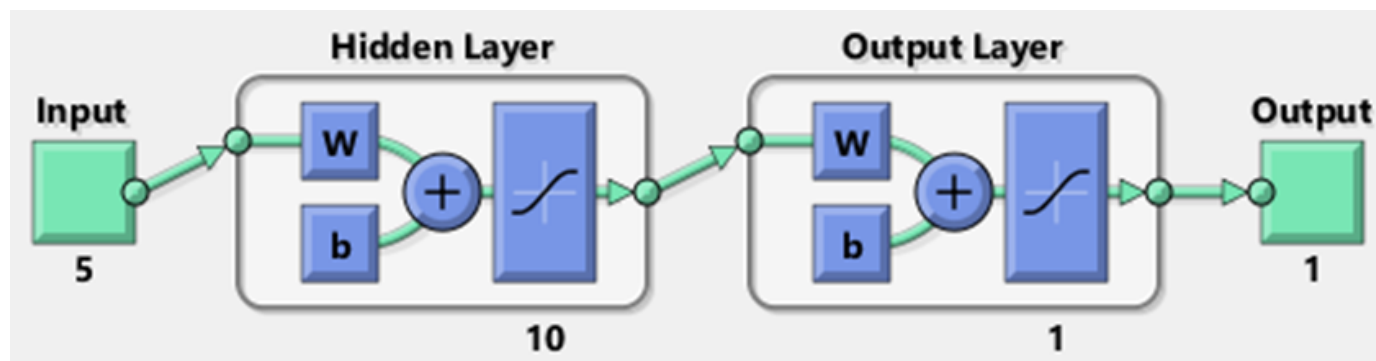


**Figure 1** A basic structure of the ANN

### ANN evaluation

ANN model was created in the MATLAB 8.4 environment, motivated by biological neurons, to perform tasks similar to those of the human brain. An MLP feed-forward ANN was employed to replicate the process through a back-propagation method (Nwosu-obieogu, 2021). The network consists of 10 hidden layers, 1 output layer representing biodiesel yield, and 5 input layers for time, catalyst dosage, temperature, agitation speed and methanol/oil ratio. Two to fifteen neurons were employed in the system's trial-and-error training to minimize the error between the hidden layer's predicted and observed values. As the number of hidden neurons increases, errors in the training data decrease, but the network's complexity also increases. The output layer neuron was assigned the linear transfer function (purelin), whereas the hidden neuron was assigned the log-sigmoid transfer function (logsig) due to the simplicity of having just one variable in the output. The 46 datasets were divided into 3 groups (70 % for training, 15 % for testing, and 15 % for validation) to evaluate the effectiveness of the ANN model. The data was standardized using min-max feature scaling to enhance the efficacy of the ANN. Figure 1 illustrates the relationship among the input, hidden and output layers of the ANN structure.

Many statistical metrics were used to calculate the generalization error and evaluate the effectiveness and functionality of the biodiesel modelling process. According to Eqns. (2) and (3), the current work utilized  $R^2$  and MSE. The

$$\text{MSE} = \frac{1}{n} \sum_{n=1}^n (d_p - O_p)^2 \quad (2)$$

$$R^2 = 1 - \frac{\sum_{n=1}^n (d_p - O_p)^2}{\sum_{n=1}^n (O_p)^2} \quad (3)$$

degree of prediction of the model is indicated by the MSE being close to 0 and the  $R^2$  being close to 1 (Onukwuli *et al.*, 2023)

## Results and Discussion

### *luffa* oil properties

Table 2 lists the physicochemical characteristics of the raw *luffa* oil seed. The oil has an acid number of 4.80 mg KOH/g and free fatty acid content of 2.50 %. These facts indicate the need for a pre-treatment step utilizing a homogeneous catalyst on the raw oil before transesterification. Nonetheless, the procedure could be inhibited by utilizing acid-modified waste marble catalysts. LSO cannot be used as a biofuel because of its high kinematic viscosity and specific gravity, which indicate that the oil has high viscosity and tends to flow slow due to resistance, which will create blockage in an internal combustion engine. The oil may be stored for a long period and cannot

**Table 2** Physicochemical characteristics of *luffa* oil

Physicochemical characteristics	<i>Luffa</i> oil
Moisture content (%)	0.25
Kinematic viscosity @ 40 °C (mm <sup>2</sup> s <sup>-1</sup> )	52.05
Refractive index @ 31oC	1.4714
Acid value(mgKOH/kg)	4.83
Free fatty acid (mgKOH/kg)	2.5
Saponification value (mgKOH/kg)	123
Peroxide value(meq/kg)	3.641
Specific gravity	0.956
Iodine value(mg I <sub>2</sub> /g)	93.51
Molecular weight(g/mol)	1907.99
Ester value(%)	87.87

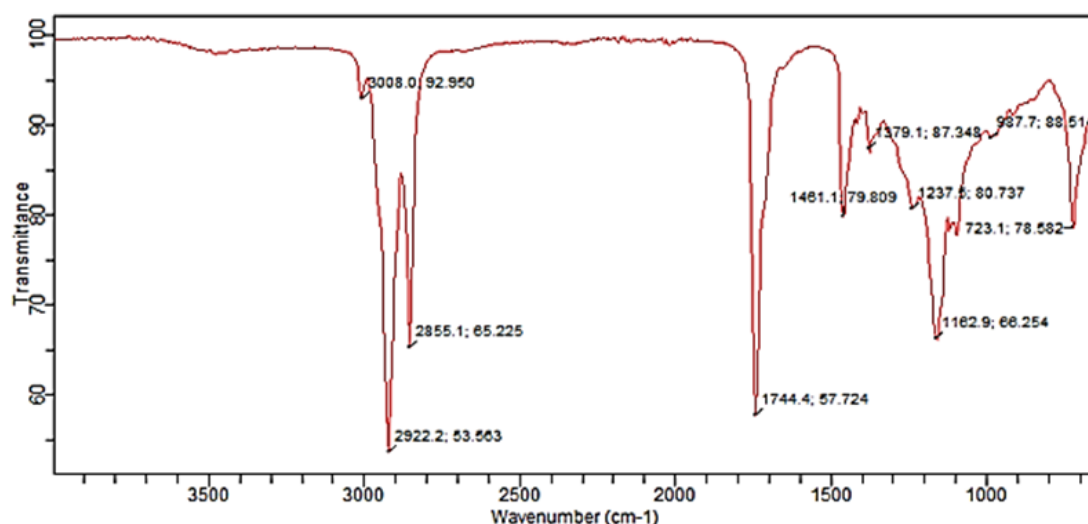


**Figure 2** FT-IR analysis of the *luffa* oil



stretching, which is the cause of the band between 3,570 and 3,656  $\text{cm}^{-1}$ . This aligns with the claims made by Onukwuli *et al.* (2023). It is possible to attribute the medium peak seen at 1982.9 and 1971.1  $\text{cm}^{-1}$  to vibrations of the C-O stretching due to the carbonates present in the waste marble.

Figure 4 displays the FTIR results for the acid-activated waste marble catalyst's characterization. The silica group is indicated by a broad peak at 2113.4  $\text{cm}^{-1}$ . The -OH stretching in the structure of the acid-activated waste marble can be attributed to the energetic band in the high-energy region at 3004.2  $\text{cm}^{-1}$ , 2855.1  $\text{cm}^{-1}$  and 2922.2  $\text{cm}^{-1}$ . The acid-activated developed catalyst made from waste marble clearly showed new peaks around 1744.4  $\text{cm}^{-1}$ , showing the stretching of sulphonic acids' S=O bonds ( $\text{SO}_3\text{-H}$ ). The analysis of this study support the reports of Sabzevar *et al.* (2021) on biodiesel production from triglyceride using ZIF-8 nanocomposite catalysts decorated with  $\text{TiO}_2$  and its use in converting used frying oil into valuable products, as well as Khan *et al.* (2021) on the formation of a heterogeneous catalyst for the development of biodiesel from wild olive oil.

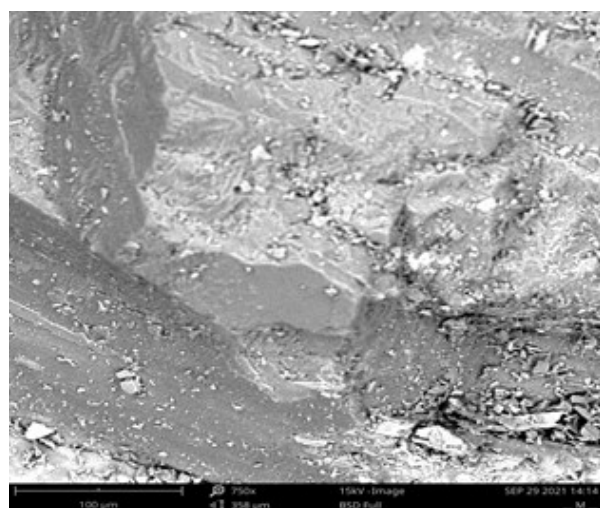
Figure 5(a) shows the structure of the untreated waste marble catalyst, while Figure 5(b) displays the structure of the waste marble catalyst after acid activation. The micrographs indicate that the number of holes and size of the pore on the clay increased in the waste marble sample created by acid. Their morphology showed pronounced agglomeration and a lack of morphological uniformity, aligning with Abdul Mutlib *et al.* (2020) on palm oil transesterification using a  $\text{SiO}_2$  sugar cane ash catalyst and Gutierrez-Lopez *et al.* (2021) on *jatropha* oil transesterification using a  $\text{NaFeTiO}_4/\text{Fe}_2\text{O}_3$  heterogeneous catalyst.

XRF evaluation was used to determine the constituents of the pure waste marble and the acid-activated waste marble catalyst, as shown in Table 4. The CaO present in the waste marble increased slightly calcination. The amount of  $\text{SO}_3$  increased from 0.856 to 6.689 weight percent. This is explained by the sizeable sulfonic group loading, which boosted catalytic activity and enabled the pure waste marble to be properly sulfonated. At the same time, the concentration of  $\text{SiO}_2$  decreased slightly after activation, with a rise in the aluminium oxide inferring the activity of the acid-activated waste marble catalyst (Yuan *et al.*, 2021).

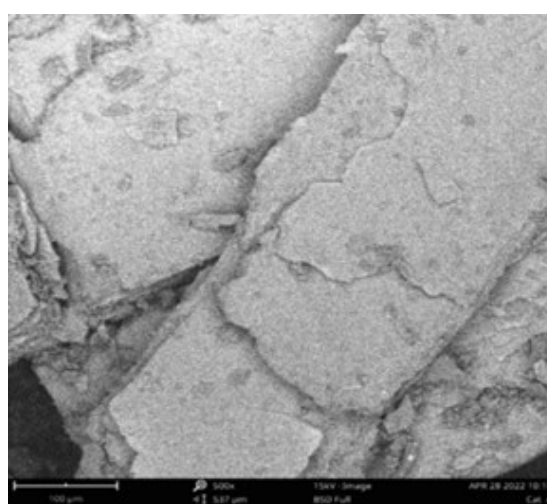
The raw waste marble had peaks at 27° and 28°, suggesting the crystalline silica structure in the waste marble. Average particle size of the HAP catalyst is 2.8  $\mu\text{m}$ , and there is no noticeable peak splitting. Crystallinity was seen from the

**Table 4** XRF for raw and acid-activated waste marble catalyst

Component	Concentration of waste marble (wt. %)	Concentration of acid-activated waste marble catalyst (wt. %)
CaO	56.025	59.352
$\text{V}_2\text{O}_5$	0.084	0.065
$\text{Cr}_2\text{O}_3$	0.053	0.041
MnO	0.148	0.162
$\text{Fe}_2\text{O}_3$	10.566	9.743
$\text{CoO}_4$	0.061	0.072
NiO	0.000	0.002
CuO	0.074	0.062
$\text{Nb}_2\text{O}_3$	0.030	0.014
$\text{MoO}_3$	0.027	0.005
$\text{WO}_3$	1.544	0.000
$\text{P}_2\text{O}_5$	0.160	0.072
$\text{SO}_3$	0.856	6.689
$\text{SiO}_2$	6.381	5.550
MgO	6.599	0.023
$\text{K}_2\text{O}$	0.287	2.414
BaO	6.492	0.241
$\text{Al}_2\text{O}_3$	4.694	5.089
$\text{Ta}_2\text{O}_5$	1.263	0.138
$\text{TiO}_2$	0.013	1.262
ZnO	2.223	0.022
$\text{Ag}_2\text{O}$	0.596	0.034
Cl	0.135	0.719
$\text{ZrO}_2$	0.303	0.075
$\text{SnO}_2$	0.227	0.230



(a)



(b)

**Figure 5** The (a) SEM for waste marble, and (b) SEM for acid-activated waste marble catalyst

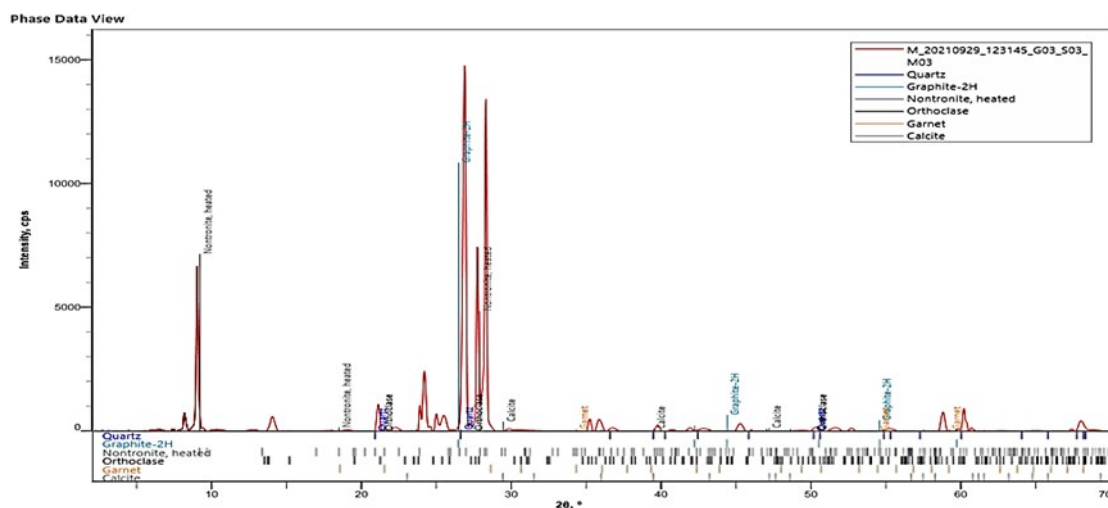


Figure 6a XRD of the raw waste marble

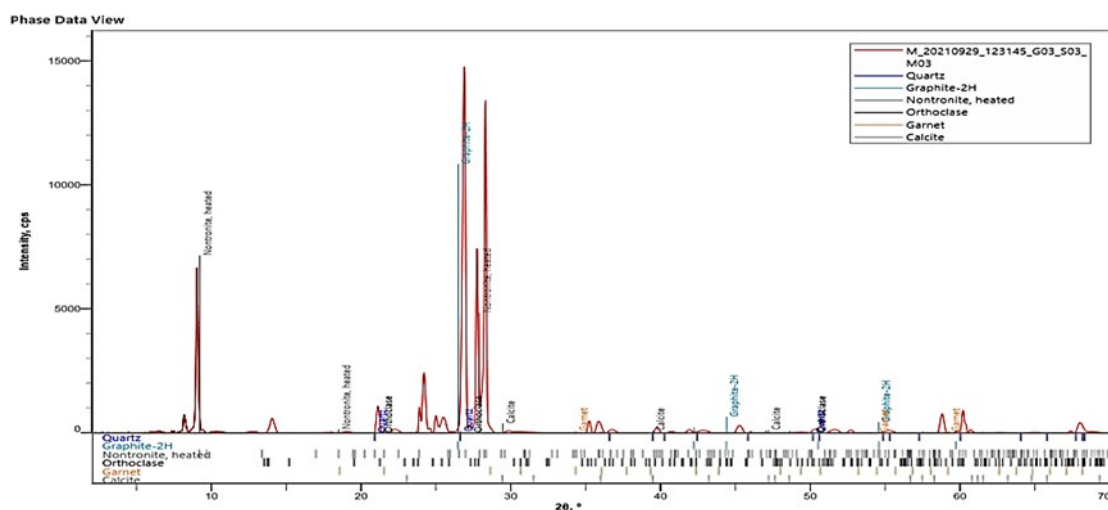


Figure 6b XRD analysis of the acid-activated marble catalyst

diffraction peaks at 27° and 28°. The oxides of metal crystal symmetry and size cause the diffraction peaks to widen and overlap. While the acid-activated waste marble catalyst in Figure 6b revealed significant peaks at 27° and 69° caused by silica's hydrogen bond breaking following the addition of acid. This demonstrated that the material had been appropriately activated, consistent with reports from Dahdah *et al.* (2021) regarding improving the fundamental qualities of Mg-Al hydrolactites for biodiesel production.

Table 5 BET evaluation of the waste marble catalyst

Parameters	Raw waste marble	Acid-activated waste marble
Total pore volume (cm <sup>3</sup> /g)	29.21	31.15
Pore size (nm)	3.146	4.283
Surface area (m <sup>2</sup> /g)	300.212	356.321

Table 5 displays the BET analyses of raw waste marble and acid-activated marble catalyst. The raw waste marble has a surface area (300.212 m<sup>2</sup>/g), a pore volume (29.21 cm<sup>3</sup>/g), and a pore size (3.146 nm). The acid-activated waste marble has a surface area of 356.321 m<sup>2</sup>/g, a pore volume of 31.15 cm<sup>3</sup>/g, and a pore diameter (4.283nm), making it more porous and

having a greater surface area compared to the raw waste marble. These unique characteristics of acid-activated waste marble support the fact that it is an effective catalyst for transesterification (Rahman *et al.*, 2021).

#### Box behken experimental luffa oil transesterification run

Table 6 shows the experimentally obtained values for the response, which is the yield. The maximum biodiesel production of 92.57 % was achieved using a catalyst dosage of 3 wt. %, a reaction duration of 2 hours, a methanol-oil molar ratio of 12:1, a temperature (60 °C), and speed of agitation (100 rpm). This illustrated how changing the process parameters affected the yield. The model equation is shown in Eqn. (4) (Foroutan *et al.*, 2021; Marzouk *et al.*, 2021). Where A denotes catalyst dosage(wt.%), B denotes methanol-oil ratio, C is time (hrs), D is the temperature (°C), and E is the speed of agitation (rpm)

#### ANOVA result

An ANOVA analysis was conducted on the model terms and their interactions in Table 7 to assess their statistical significance. The linear terms, quadratic and interaction terms has a significant impact on the yield as indicated by the big f-value and accompanying p-values. The outcome indicated the strong correlation of all variables in the model. Yahya *et al.* (2020) have shown comparable results on enhancing biodiesel

$$\text{Biodiesel yield (\%)} = 86.70 + 2.09A + 4.61B - 3.00C + 0.62D - 0.60E + 1.33AB - 2.05AV + 1.55AD - 3.50AE + 5.75BC - 1.13BD - 7.00BE - 1.46CD - 4.04CE - 2.02DE - 5.02A^2 - 1.97B^2 - 5.69C^2 - 5.48D^2 - 2.89E^2 \quad (4)$$

**Table 6** *luffa* oil transesterification experimental run using acid waste marble catalyst

Runs	Catalyst conc. wt. %	Meth/oil ratio	Time hours	Temperature °C	Agitation speed rpm	Biodiesel yield %
1	3	4	2	60	100	71.59
2	3	8	3	60	500	69.87
3	3	4	2	40	300	72.27
4	5	4	2	60	300	75.18
5	3	8	1	60	500	83.95
6	1	4	2	60	300	73.71
7	1	8	3	60	300	73.2
8	5	8	3	60	300	73.22
9	3	12	3	60	300	86.54
10	3	4	2	60	500	86.64
11	5	8	1	60	300	83.33
12	3	8	2	40	500	78.51
13	5	8	2	80	300	80.97
14	3	4	3	60	300	65.06
15	5	8	2	40	300	76.44
16	1	8	2	80	300	73.49
17	5	8	2	60	100	85.05
18	3	8	1	40	300	76.77
19	1	8	2	60	100	73.93
20	3	8	2	60	300	86.7
21	3	12	2	60	500	79.62
22	3	12	2	60	100	92.57
23	3	8	1	60	100	77.83
24	1	8	2	40	300	75.17
25	1	12	2	60	300	81.04
26	3	12	2	80	300	83.43
27	3	8	2	60	300	86.7
28	3	8	2	60	300	86.7
29	3	8	3	60	100	79.89
30	3	8	2	40	100	76.42
31	3	8	2	60	300	86.7
32	3	8	1	80	300	80.75
33	1	8	2	60	500	78.98
34	3	8	3	40	300	73.56
35	5	12	2	60	300	87.81
36	5	8	2	60	500	76.1
37	3	12	1	60	300	81.05
38	3	12	2	40	300	84.51
39	3	8	3	80	300	71.94
40	3	8	2	80	100	81.64
41	1	8	1	60	300	75.11
42	3	8	2	60	300	86.7
43	3	4	2	80	300	75.71
44	3	8	2	60	300	86.7
45	3	8	2	80	500	75.65
46	3	4	1	60	300	82.57

from used cooking oil with Fe-clay K10 catalyst using RSM. The model is highly reliable and effective for optimization, indicated by the standard deviation of 0.86, mean of 79.38, coefficient of variation of 1.08 %, F-value of 107.23, significance level of 0.05, and precision of 48.991. The model's lack of fit was 18.38, indicating a statistically minor discrepancy; therefore, reinforcing the model's strong fit. The  $R^2$  (0.9885), adjusted  $R^2$  (0.9793), and predicted  $R^2$  (0.9539) coefficients were utilized to evaluate the fitness of the polynomial model, showing that the experimental data aligns well with the expected data.

### Parametric analysis

Figure 9a depicted the correlation between catalyst dosage and methanol-oil ratio on the yield. Increasing catalyst dosage and methanol-oil ratio were found to increase the yield. However, increasing time and catalyst dosage reduced the yield in Figure 9b. In Figure 9c, increasing catalyst dosage and temperature decreased the yield. Additionally, increasing catalyst dosage (wt.%) and agitation speed decreased the yield in Figure 9d. This trend may be attributed to the surplus catalyst causing rapid feedstock conversion. Figure 9e shows that a higher

methanol-oil ratio and longer reaction time resulted in a lower biodiesel yield. Figure 9f shows that raising the methanol-oil ratio and temperature resulted in a higher biodiesel output. Figure 9g shows that higher methanol-oil ratio and speed of agitation led to an increase in the yield. In Figure 9i, higher time and speed of agitation led to a rise in biodiesel output. Figure 9j showed that raising the temperature led to an increase in the biodiesel output. As the time and temperature rose, the methanol evaporated, resulting in a higher yield. The 3D figures demonstrate that process parameters affect the response, with the quadratic terms having a more substantial impact on the yield compared to the interaction terms. This observation aligns with the study conducted by Foroutan et al. (2021) on waste chicken fat biodiesel utilizing a waste glass catalyst.

### Optimization of luffa oil transesterification

Figure 10 shows the optimization of the process via RSM tool. The optimum yield of 94.0488 % was obtained via a catalyst conc. of 3 wt.%, a methanol-oil ratio of 12:1, a time of 2 hours, a reaction temperature of 600 °C, and a speed of agitation of 100 rpm with the desirability of 1.000; this aligns with the observed biodiesel yield of 92.57 %, which was obtained at the

**Table 7** ANOVA result of transesterification of *luffa* oil using acid-activated waste marble catalyst

Source	Sum of Squares	df	Mean Square	F Value	Prob > F
Model	1576.95	20	78.85	107.23	< 0.0001
A-Catalyst conc.	70.02	1	70.02	95.22	< 0.0001
B-meth/oil ratio	340.77	1	340.77	463.43	< 0.0001
C-time	144.48	1	144.48	196.49	< 0.0001
D-temperature	6.16	1	6.16	8.38	0.0078
E-agitation speed	5.76	1	5.76	7.83	0.0097
AB	7.02	1	7.02	9.55	0.0049
AC	16.81	1	16.81	22.86	< 0.0001
AD	9.64	1	9.64	13.11	0.0013
AE	49.00	1	49.00	66.64	< 0.0001
BC	132.25	1	132.25	179.85	< 0.0001
BD	5.11	1	5.11	6.95	0.0142
BE	196.00	1	196.00	266.55	< 0.0001
CD	7.84	1	7.84	10.66	0.0032
CE	65.12	1	65.12	88.57	< 0.0001
DE	16.32	1	16.32	22.20	< 0.0001
A <sup>2</sup>	219.91	1	219.91	299.07	< 0.0001
B <sup>2</sup>	33.95	1	33.95	46.17	< 0.0001
C <sup>2</sup>	282.95	1	282.95	384.79	< 0.0001
D <sup>2</sup>	261.90	1	261.90	356.18	< 0.0001
E <sup>2</sup>	73.09	1	73.09	99.40	< 0.0001
Residual	18.38	25	0.74		
Lack of Fit	18.38	20	0.92		
Pure Error	0.000	5	0.000		
Cor Total	1595.33	45			
Std. Dev.	0.86	R-Squared	0.9885		
Mean	79.38	Adj R-Squared	0.9793		
C.V. %	1.08	Pred R-Squared	0.9539		
PRESS	73.53	Adeq Precision	48.991		

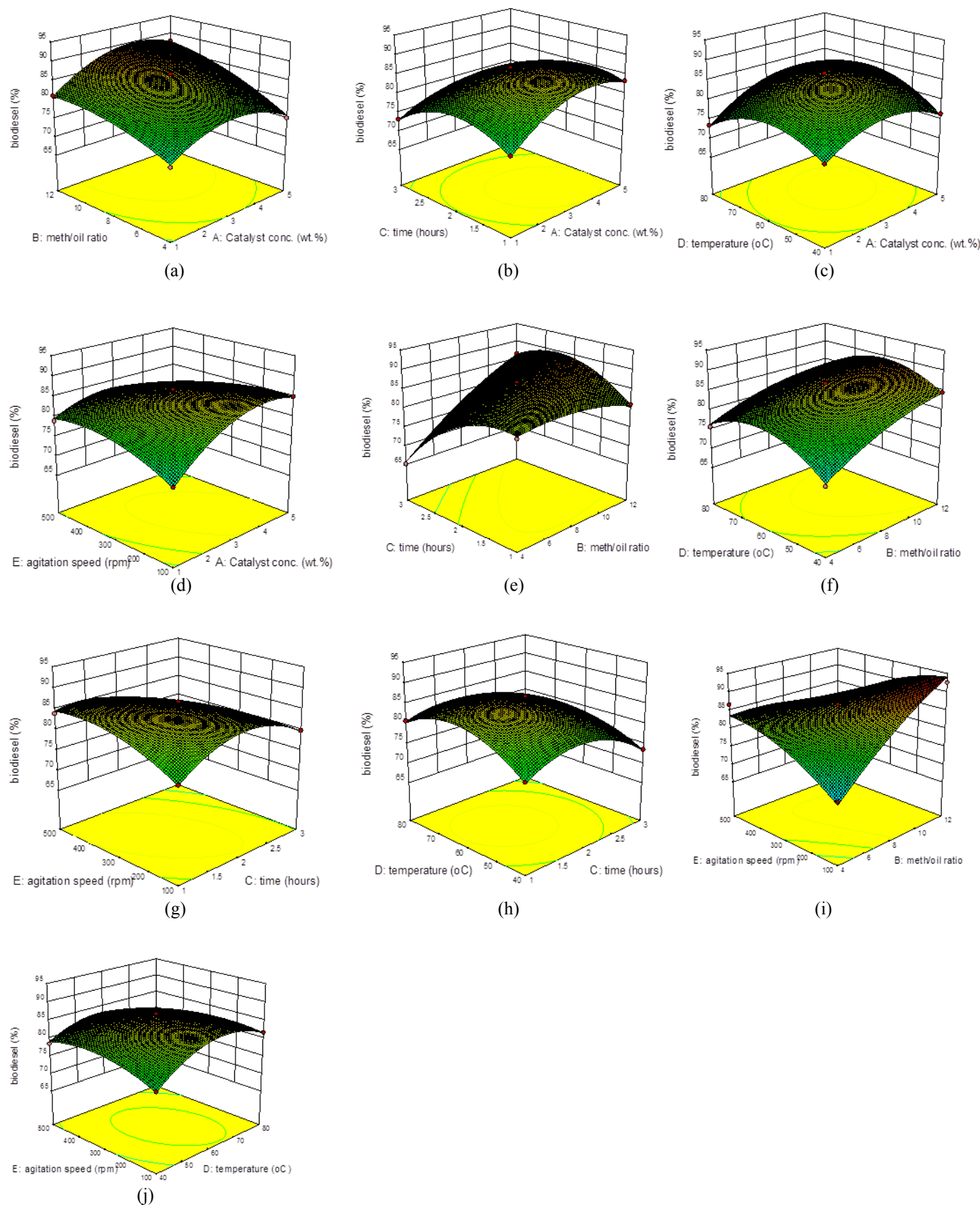


**Figure 9** 3D surface plots of *luffa* oil biodiesel yield catalysed by activated waste marble catalyst: **a.** methanol-oil ratio and catalyst concentration, **b.** catalyst concentration and time, **c.** temperature and catalyst concentration, **d.** catalyst concentration and agitation speed, **e.** methanol-oil ratio and time, **f.** methanol-oil ratio and temperature, **g.** agitation speed and methanol, **h.** temperature and time, **i.** time and agitation speed, and **j.** temperature and agitation speed

same conditions (Ajala *et al.*, 2015; Marzouk *et al.*, 2021).

**Table 8** Model performance for ANN

Algorithm	MSE	R <sup>2</sup>
Levenberg-Marquardt	0.063311	9.9921E-1
Bayesian regularization	1.6501	9.827E-1
Scaled Conjugate Gradient	1.6922	9.9705E-1

### ANN model simulation

The feed-forward, back-propagation algorithms formed the basis for creating the ANN-based model. Ten neurons constitute the hidden layer. The best algorithm for biodiesel yield is Levenberg-Marquardt because it has the lowest MSE (0.063311) and highest R<sup>2</sup>(9.9921E-1) amongst other algorithms as shown in Table 8. As illustrated in Figures 11 and 12, the regression coefficient and mean squared error suggest that the ANN model successfully predicted the *luffa* oil transesterification process. The effectiveness of the expected ANN model conforms with the findings from Suresh *et al.* (2021) on ANN prediction of ultrasonic-assisted production

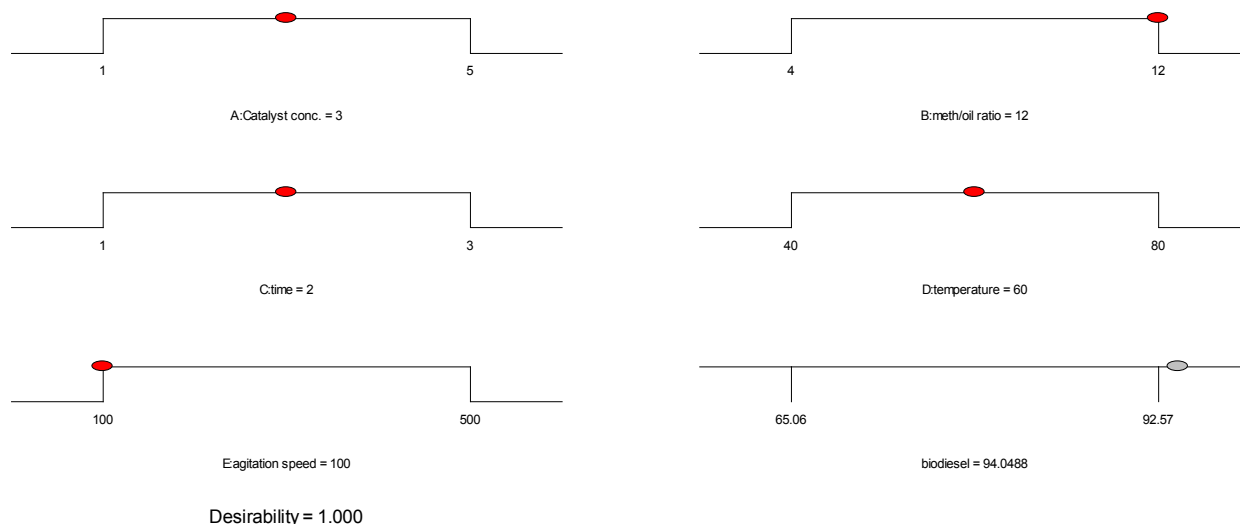
of biodiesel from pig tallow using green CuO nanocatalyst and Foroutan *et al.* (2021) on ANN application in waste chicken fat transesterification using waste glass catalyst.

**Table 10** comparison of RSM and ANN performance

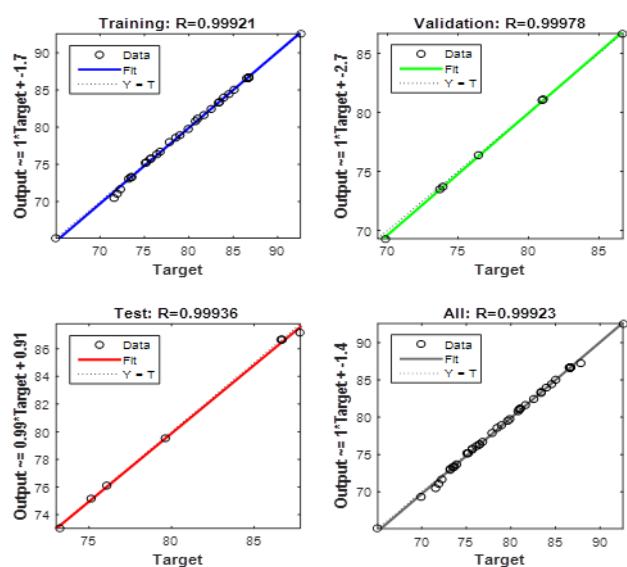
Performance indicators	RSM	ANN
R <sup>2</sup>	0.9885	9.9921E-1
MSE	0.86	0.063311

Table 9 shows the observed and RSM-predicted values for biodiesel production with the simulated ANN values from the Levenberg Marquardt technique. The highest observed biodiesel production (92.57 %) and the predicted yields (94.0487 %) and (91.1768 %) from RSM and ANN, respectively, are in agreement. This coincides with the reports from Foroutan *et al.* (2021) on waste chicken fat transesterification.

Table 10 compares the desired results for RSM and ANN using statistical criteria (R<sup>2</sup> and MSE) to determine the models' dependability. Both the RSM's (0.9885) and the ANN's (9.921E-1) coefficients of determination (R<sup>2</sup>) were found to be



**Figure 10** Optimum conditions for *luffa* oil transesterification with minimized error



**Figure 11** ANN graph

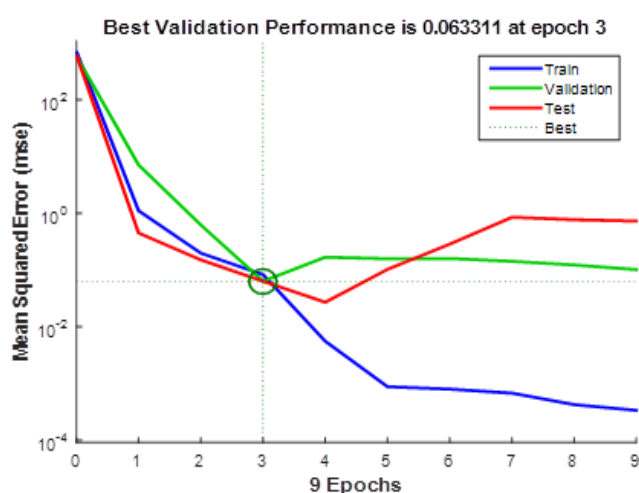


**Figure 12** Mean squared error for *luffa* oil transesterification

**Table 9** BBD predictive model adequacy

<b>Runs</b>	<b>Experimental predicted biodiesel yield</b>	<b>RSM predicted biodiesel yield</b>	<b>ANN predicted biodiesel yield</b>
1	71.59	70.8187	77.4682
2	69.87	70.4721	68.0218
3	72.27	72.884	72.0465
4	75.18	75.8598	75.7821
5	83.95	84.5521	85.3356
6	73.71	74.326	72.9708
7	73.2	72.9394	70.4563
8	73.22	73.0231	73.5682
9	86.54	86.3937	84.957
10	86.64	83.6188	80.4289
11	83.33	83.1331	81.5986
12	78.51	79.1273	77.599
13	80.97	80.4671	78.7083
14	65.06	65.6637	67.0024
15	76.44	76.1208	75.9656
16	73.49	73.1783	69.3725
17	85.05	84.9781	84.1702
18	76.77	76.5123	75.2663
19	73.93	73.7944	75.3017
20	86.7	86.7	85.3758
21	79.62	78.8487	82.849
22	92.57	94.0487	91.1768
23	77.83	77.6821	79.1772
24	75.17	75.0421	76.1662
25	81.04	80.906	73.0519
26	83.43	83.3552	83.1103
27	86.7	86.7	85.3758
28	86.7	86.7	85.3758
29	79.89	79.7421	77.8016
30	76.42	76.2873	76.4653
31	86.7	86.7	85.3758
32	80.75	80.5535	80.5277
33	78.98	79.5944	78.9906
34	73.56	73.3023	74.2899
35	87.81	87.7398	87.4689
36	76.1	76.7781	84.9625
37	81.05	80.9038	85.1878
38	84.51	84.374	83.4261
39	71.94	71.7435	67.299
40	81.64	81.5685	79.9718
41	75.11	74.8494	77.3897
42	86.7	86.7	85.3758
43	75.71	76.3852	75.5544
44	86.7	86.7	85.3758
45	75.65	76.3285	75.7399
46	82.57	83.1737	79.318

very close to 1. The MSE of RSM (0.86) and ANN (0.063311) are close to zero simultaneously, showing that both models can forecast the transesterification process. Nonetheless, ANN evaluated the process more accurately than RSM, reflected in the higher  $R^2$  and lower MSE of ANN compared to RSM (Betiku *et al.*, 2016; Foroutan *et al.*, 2021).

The optimal conversion of a triglyceride of *luffa* oil is shown using FT-IR in Figure 19. The bending peaks of the O=C=O group are aligned to the IR peaks at 1237.5-1744.4  $\text{cm}^{-1}$  for LSO biodiesel. The C-H stretching of the alkyl group and the C=O stretching of the esters group, respectively, are attributed to the two bands for *luffa* oil that fall within the range of 2855.1-3011.7  $\text{cm}^{-1}$  and peak at 1744.4  $\text{cm}^{-1}$  on the IR spectra of the catalyst. These bands developed as a result of the oils' unconverted triglycerides. The peak represents O-CH<sub>3</sub> at 1159.2  $\text{cm}^{-1}$ , which indicates that methyl ester was formed in the band. (Nadeem *et al.*, 2021; Karmakar *et al.*, 2020).

It can be shown that the triglyceride of *luffa* oil was converted to methyl esters in Figure 20 after being subjected to an acid-activated waste marble catalyst. The highest peaks show that methyl ester is present (18.006). However, the lower peaks shows triglyceride. (Naveenkumar and Baskar, 2021).

### Biodiesel physicochemical properties

The physicochemical properties of biodiesel made from *luffa* oil. The biodiesel has a moisture content (0.019 %) and a

specific gravity (0.8733), which aligns with previous studies and falls within the desired range. The biodiesel's acid value of 3.312 and free fatty acid (1.656) met the ASTM specifications for biodiesel, which helps prevent corrosion and deposits in the engine. The iodine value of 3.24 suggests that unsaturated fatty acid triglycerides have undergone transesterification. Higher cetane numbers correspond to shorter delay intervals and increased fuel combustibility. Low cetane number fuels present difficulties in initiating engine combustion, resulting in smoke emissions. The biodiesel's high cetane number of 54.39, exceeding the ASTM limit of 47, suggests low emissions and clean combustion due to the catalyst utilized in the transesterification process. The aniline point, flash point, diesel index, gross calorific value and cloud point of the *luffa* oil biodiesel were all within the ASTM criteria for methyl ester. The kinematic viscosity of the biodiesel, 5.93  $\text{mm}^2/\text{s}$ , falls within the ASTM range of 1.9-6.0, suggesting that it has good flowability. (Nadeem *et al.*, 2021; Tamoradi *et al.*, 2021).

### Conclusions

Regarding RSM and ANN, this work successfully modelled the transesterification of *luffa* oil. The oil can be applied in biodiesel production, according to the results of the characterization of the *luffa* oil and the biodiesel produced. The waste marble was suitably characterized by FT-IR, SEM, XRD, XRF, and BET. While *luffa* oil and the developed

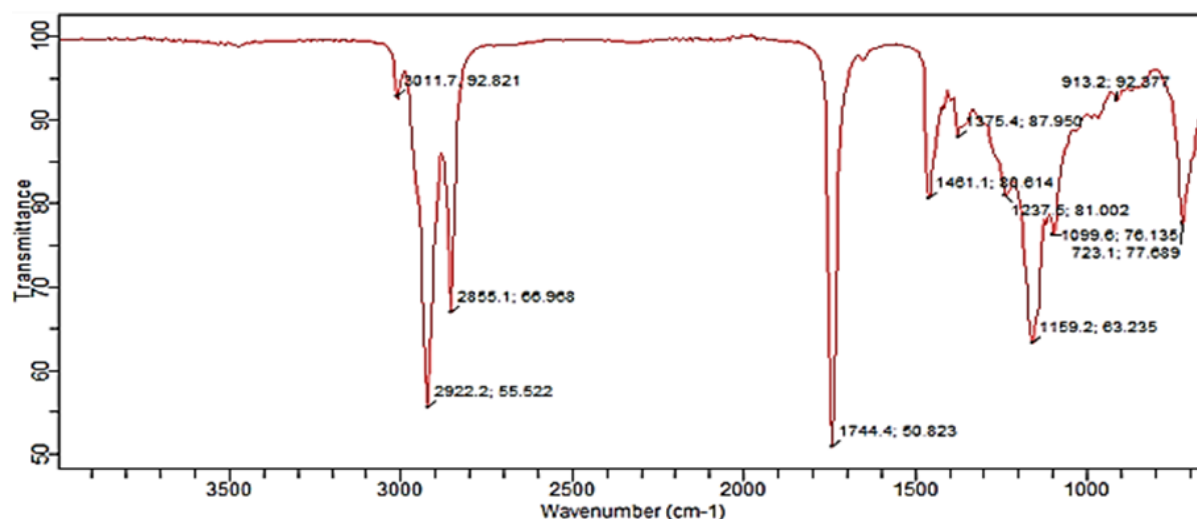


Figure 19 FT-IR analysis of *luffa* oil biodiesel

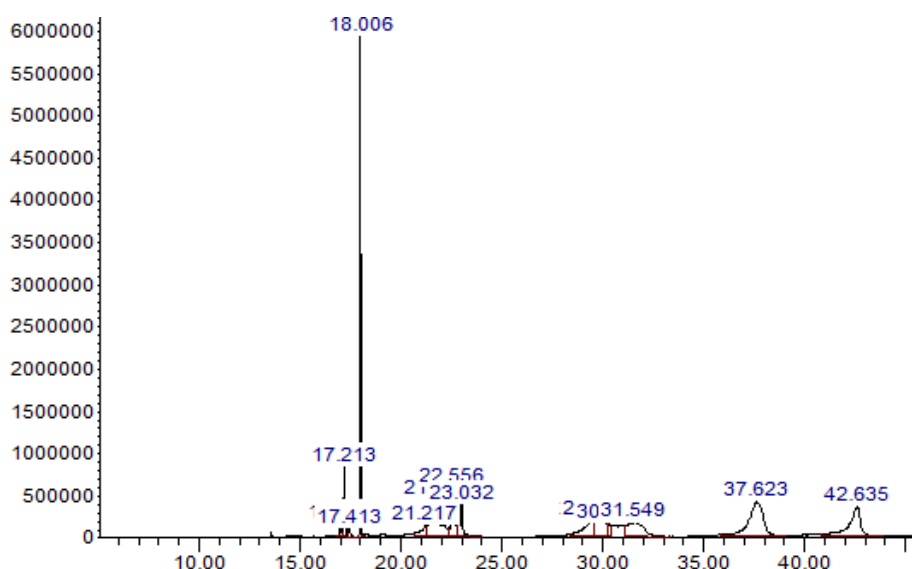


Figure 20 GCMS analysis of optimal LSO biodiesel

biodiesel was characterised with FTI-R and GCMS. Based on the ANOVA results, catalyst concentration, methanol/mol ration and time significantly impacted the biodiesel yield than other parameters.

The results demonstrated the effectiveness of the prediction models of the *luffa* oil transesterification process; however, comparisons between the two techniques revealed that the ANN model ( $R^2 = 9.9921E-1$ ,  $MSE = 0.063311$ ) outperformed the RSM ( $R^2 = 0.9885$ ,  $MSE = 0.86$ ). The optimum biodiesel yield of 92.57% validated the values predicted by RSM (94.0487 %) and ANN (91.1768 %).

## Acknowledgement

For their assistance with this research, the authors appreciate the team at the Chemical Analysis Laboratory, Michael Okpara University of Agriculture, Umudike.

## Conflict of Interest Declaration

The authors have no conflict of interest to declare.

## References

- Abdul Mutalib, A. A., Ibrahim, M. L., Matmin, J., Kassim, M. F., Mastuli, M. S., Taufiq-Yap, Y. H., Shohaimi, N. A. M., Islam, A., Tan, Y. H., and Kaus, N. H. M. (2020). SiO<sub>2</sub>-Rich Sugar cane bagasse ash catalyst for transesterification of palm oil. *Bioenergy Research*, 13(3), pp. 986–997. <https://doi.org/10.1007/s12155-020-10119-6>
- Adewuyi, A., Oderinde, R. A., Rao, B. V. S. K., Prasad, R. B. N., and Anjaneyulu, B. (2012). Blighia unijugata and luffa cylindrica seed oils: Renewable sources of energy for sustainable development in rural Africa. *BioEnergy Research*, 5, pp. 713-718.
- Ajala, E. O., Aberuagba, F., Olanayan, A. M., and Onifade, K. R. (2015). Optimization of solvent extraction of shea butter (*Vitellaria paradoxa*) using response surface methodology and its characterization. *J Food Sci Technol*, 23(7), pp. 457-467. <https://doi.org/10.1007/s13197-015-2033-7>
- Balajii, M., and Niju, S. (2020). Banana peduncle – A green and renewable heterogeneous base catalyst for biodiesel production from Ceiba pentandra oil. *Renewable Energy*, 146, pp. 2255–2269. <https://doi.org/10.1016/j.renene.2019.08.062>
- Bargole, S. S., Singh, P. K., George, S., and Saharan, V. K. (2021). Valorisation of low fatty acid content waste cooking oil into biodiesel through transesterification using a basic heterogeneous calcium-based catalyst. *Biomass and Bioenergy*, 146, pp. 105-124. <https://doi.org/10.1016/j.biombioe.2021.105984>
- Bedir, Ö., and Doğan, T. H. (2021). Use of sugar industry waste catalyst for biodiesel production. *Fuel*, 286, 14595. <https://doi.org/10.1016/j.fuel.2020.119476>
- Betiku, E., Odude, V. O., Ishola, N. B., Bamimore, A., Osunleke, A. S., and Okeleye, A. A. (2016). Predictive capability evaluation of RSM, ANFIS and ANN: A case of reduction of high free fatty acid of palm kernel oil via esterification process. *Energy Conversion and Management*, 124, pp. 219–230. <https://doi.org/10.1016/j.enconman.2016.07.030>
- Chinweuba, A. J. (2017). Potential industrial applications of luffa cylindrica seed oil. *Journal of Scientific and Engineering Research*, 4(3), pp. 66-68
- Dahdah, E., Estephane, J., Taleb, Y., El Khoury, B., El Nakat, J., and Aouad, S. (2021). The role of rehydration in enhancing the basic properties of Mg–Al hydrotalcites for biodiesel production. *Sustainable Chemistry and Pharmacy*, 22, 100487.
- Esonye, C., Dominic, O., and Uwaoma, A. (2019). Characterization and oxidation modeling of oils from *Prunus amygdalus*, *Dyacrodes edulis* and *Chrysophyllum albidium*. *Industrial Crops and Products*, 128(October 2018), pp. 298–307. <https://doi.org/10.1016/j.indcrop.2018.11.029>
- Foroutan, R., Mohammadi, R., and Ramavandi, B. (2021). Waste glass catalyst for biodiesel production from waste chicken fat: Optimization by RSM and ANNs and toxicity assessment. *Fuel*, 291(December 2020), pp. 218-227. <https://doi.org/10.1016/j.fuel.2021.120151>
- Foroutan, R., Peighambaroust, S. J., Mohammadi, R., Ramavandi, B., and Boffito, D. C. (2021). One-pot transesterification of non-edible *Moringa oleifera* oil over a MgO/K<sub>2</sub>CO<sub>3</sub>/HAp catalyst derived from poultry skeletal waste. *Environmental Technology and Innovation*, 21, pp. 234-251. <https://doi.org/10.1016/j.eti.2020.101250>
- Ibeto, C. N., Okoye, C. O. B., and Ofoefule, A. U. (2012). Comparative study of the physicochemical characterization of some oils as potential feedstock for biodiesel production. *International Scholarly Research Notices*, 12, pp. 1-10.
- Idris, N. A., Lau, H. L. N., Wafti, N. S. A., Mustaffa, N. K., and Loh, S. K. (2021). Glycerolysis of Palm Fatty Acid Distillate (PFAD) as Biodiesel Feedstock Using Heterogeneous Catalyst. *Waste and Biomass Valorization*, 12(2), pp. 735–744. <https://doi.org/10.1007/s12649-020-00995-6>
- Karmakar, B., Samanta, S., and Halder, G. (2020). Delonix regia heterogeneous catalyzed two-step biodiesel production from *Pongamia pinnata* oil using methanol and 2-propanol. *Journal of Cleaner Production*, 255, pp. 1203-1213. <https://doi.org/10.1016/j.jclepro.2020.120313>
- Laskar, I. B., Gupta, R., Chatterjee, S., Vanlalveni, C., and Rokhum, L. (2020). Taming waste: Waste *Mangifera indica* peel as a sustainable catalyst for biodiesel production at room temperature. *Renewable Energy*, 161, pp. 207–220. <https://doi.org/10.1016/j.renene.2020.07.061>
- Mostafa Marzouk, N., Abo El Naga, A. O., Younis, S. A., Shaban, S. A., El Torgoman, A. M., and El Kady, F. Y. (2021). Process optimization of biodiesel production via esterification of oleic acid using sulfonated hierarchical mesoporous ZSM-5 as an efficient heterogeneous catalyst. *Journal of Environmental Chemical Engineering*, 9(2), pp.105-125. <https://doi.org/10.1016/j.jece.2021.105035>
- Nadeem, F., Bhatti, I. A., Ashar, A., Yousaf, M., Iqbal, M., Mohsin, M., Nisar, J., Tamam, N., and Alwadai, N. (2021). Eco-benign biodiesel production from waste cooking oil using eggshell derived MM-CaO catalyst and condition optimization using RSM approach. *Arabian Journal of Chemistry*, 14(8), pp. 103-113. <https://doi.org/10.1016/j.arabjc.2021.103263>
- Naveenkumar, R., and Baskar, G. (2021). Process optimization, green chemistry balance and technoeconomic analysis of biodiesel production from castor oil using heterogeneous nanocatalyst. *Bioresource Technology*, 320, pp. 124-137. <https://doi.org/10.1016/j.biortech.2020.124347>
- Nitsos, C. K., Lazaridis, P. A., Mach-Aigner, A., Matis, K. A., and Triantafyllidis, K. S. (2019). Enhancing lignocellulosic biomass hydrolysis by hydrothermal pretreatment, extraction of surface lignin, wet milling and production of cellulolytic enzymes. *ChemSusChem*, 12(6),

- pp. 1179–1195. <https://doi.org/10.1002/cssc.201802597>.
- Nwosu-obieogu, K. (2021). Artificial Neural Network Predictive Modelling of luffa cylindrica Seed Oil Antioxidant Yield. *Gazi University Journal of Science Part A: Engineering and Innovation*, 8(4), pp. 494-504.
- Nwosu-Obieogu, K., Dzarma, G. W., Ugwuodo, C. B., Chiemenem, L. I., and Akatobi, K. N. (2022). Luffa seed oil extraction: response surface and neuro-fuzzy modelling performance evaluation and optimization. *Process Integration and Optimization for Sustainability*, pp. 1-14.
- Nwosu-Obieogu, K., and Umunna, M. (2021). Rubber seed oil epoxidation: experimental study and soft computational prediction. *Annals of the Faculty of Engineering Hunedoara-International Journal of Engineering*, (4), pp. 12-25.
- Oke, E. O., Nwosu-Obieogu, K., Okolo, B. I., Adeyi, O., Omotoso, A. O., and Ude, C. U. (2021). Hevea brasiliensis oil epoxidation: hybrid genetic algorithm–neural fuzzy–Box–Behnken (GA–ANFIS–BB) modelling with sensitivity and uncertainty analyses. *Multiscale and Multidisciplinary Modeling, Experiments and Design*, 4, pp. 131-144.
- Onukwuli, O. D., Joseph, E., Nonso, U. C. and Nwosu-obieogu., K. (2022). Improving heterogeneous catalysis for biodiesel production process. *Cleaner Chemical Engineering*, 3, 100038.
- Onukwuli, O. D., Nwosu-obieogu, K., Joseph, E. and Nonso, U. C. (2023). Soft computing prediction of linseed oil transesterification process via clay-doped barium chloride catalyst. *Process Integration and Optimization for Sustainability*, pp. 1-26. <https://doi.org/10.1016/j.fuel.2020.119586>.
- Qasemi, Z., Jafari, D., Jafari, K., and Esmaeili, H. (2021). Heterogeneous aluminum oxide/calcium oxide catalyzed transesterification of mespilus germanica triglyceride for biodiesel production. *Environmental Progress and Sustainable Energy*, 4(2), pp. 1–12. <https://doi.org/10.1002/ep.13738>.
- Rahman, M. M., Hassan, T., Rabbi, M. F., Shakil, M. F., and Khan, M. A. (2021). Transesterification of vegetable oil with ethanol using different catalysts. In *AIP Conference Proceedings* 2324(1). AIP Publishing.
- Sabzevar, A., Ghahramaninezhad, M., and Niknam Shahrak, M. (2021). Enhanced biodiesel production from oleic acid using TiO<sub>2</sub>-decorated magnetic ZIF-8 nanocomposite catalyst and its utilization for used frying oil conversion to valuable product. *Fuel*, 288, 119586.
- Sahu, O. (2021). Characterisation and utilization of heterogeneous catalyst from waste rice-straw for biodiesel conversion. *Fuel*, 287, pp. 119-243. <https://doi.org/10.1016/j.fuel.2020.119543>
- Sai, A., Niju, S., Meera, K.M. and Anantharaman, N. (2019). Optimization and modeling of biodiesel production using fluorite as a heterogeneous catalyst. *Energy Sources, Part A: Recovery, Utilization and Environmental Effects*, 41 (15), pp. 1862–1878. <https://doi.org/10.1080/15567036.2018.1549165>
- Shobhana-Gnanaserkhar, Asikin-Mijan, N., AbdulKareem-Alsultan, G., Sivasangar-Seenivasagam, Izham, S. M., and Taufiq-Yap, Y. H. (2020). Biodiesel production via simultaneous esterification and transesterification of chicken fat oil by mesoporous sulfated Ce supported activated carbon. *Biomass and Bioenergy*, 141, pp. 105-122. <https://doi.org/10.1016/j.biombioe.2020.105714>
- Suresh, T., Sivarajasekar, N., and Balasubramani, K. (2021). Enhanced ultrasonic assisted biodiesel production from meat industry waste (pig tallow) using green copper oxide nanocatalyst: Comparison of response surface and neural network modelling. *Renewable Energy*, 164, pp. 897–907. <https://doi.org/10.1016/j.renene.2020.09.112>
- Tamoradi, T., Kiasat, A. R., Veisi, H., Nobakht, V., Besharati, Z., and Karmakar, B. (2021). MgO doped magnetic graphene derivative as a competent heterogeneous catalyst producing biofuels via transesterification: Process optimization through Response Surface Methodology (RSM). *Journal of Environmental Chemical Engineering*, 9 (5), pp. 106-129. <https://doi.org/10.1016/j.jece.2021.106009>
- Ude, C. N., Onukwuli, O. D., Okoye, C. N., Anisiji, O. E., Atuanya, C. U., Menkiti, C., Onukwuli, O. D., Okoye, C. N., Anisiji, O. E., and Atuanya, C. U. (2017). Performance evaluation of cottonseed oil methyl esters produced using CaO and prediction with an artificial neural network. *7269 (4)*, pp.42-56. <https://doi.org/10.1080/17597269.2017.1345355>
- Wang, A., Quan, W., Zhang, H., Li, H., and Yang, S. (2021). Heterogeneous ZnO-containing catalysts for efficient biodiesel production. *RSC Advances*, 11(33), pp. 20465–20478. <https://doi.org/10.1039/d1ra03158a>
- Yahya, S., Wahab, S. K. M., and Harun, F. W. (2020). Optimization of biodiesel production from waste cooking oil using Fe-Montmorillonite K10 by response surface methodology. *Renewable Energy*, 157, pp. 164-172.
- Zhang, Y., Niu, S., Han, K., Li, Y., and Lu, C. (2021). Synthesis of the SrO–CaO–Al<sub>2</sub>O<sub>3</sub> trimetallic oxide catalyst for transesterification to produce biodiesel. *Renewable Energy*, 168, pp. 981–990. <https://doi.org/10.1016/j.renene.2020.12.132>